Mestrado Integrado em Engenharia Química

CFD in Industrial Processes: Stirred Tank Flow and Power Assessment

Tese de Mestrado

Desenvolvida no âmbito

Projecto de Desenvolvimento em Ambiente Empresarial

Pedro Miguel Meirinhos Afonso

FLUIDINOVA
ENGENHARIA DE FLUIDOS

CFDapi

Universidade do Porto
Faculdade de Engenharia
FEUP

Departamento de Engenharia Química

Responsável FEUP: **José Carlos Brito Lopes**

Responsável FLUIDINOVA: **Renato Gomes de Sousa**

Fevereiro 2008

To my Parents. To my friends. To Bragança, my homeland.

Acknowledgements

The ambience of near academic freedom, the facilities and the friendly atmosphere at the Fluidinova office, all have contributed in no small measure to the conclusion of this work.

I am particularly grateful for having had the guidance and patience of Doctor Renato Sousa, who supervised this work. It has been a learning experience for me to observe him carring out a variety of roles.

I would like to express my special gratitude to Hugo Campelo, Joana Cardoso and Paulo Gomes for introducing me to the immeasurable world of CFD and make me understand how it can test a man's patience.

I am grateful to my colleagues at Fluidinova, with whom I worked on different industrial projects, for their cooperation in many matters.

In particular, I am grateful to Claudio Fonte and Carlos Fonte with whom working is never the same, Paulo Quadros, António Azevedo and Alexandre Beirão for always providing a good and inspiring work environment, António Gouveia for all the software and hardware solutions and/or updates and Doctor André Teixeira for his technical contributions either in a direct or indirect way, helping me to collect the required information for this work.

A special thanks to Daniela Correia and Marisa Rodrigues who entered FLUIDINOVA at the same time as me, also master students, my most sincere acknowledgement for these five months.

This work was improved wherever their suggestions were incorporated.

I owe much to Professor Madalena Dias and Professor José Carlos Lopes at FEUP, for their considerable advice and guidance during preparation of this thesis.

Finally, I wish to thank my girlfriend, Ana, for her patience, understanding and enthusiastic support, which carried me through this arduous internship process.

Abstract

This thesis aims to study the effect of a second impeller on the enhancement of the solid/liquid mixture in an industrial stirred tank by analyzing the flow patterns and their effect on the power consumption. The simulation parameters were continually tuned up until no enhancement on the predicted power was achieved. The Moving Reference Frame (MRF) model has been found to give adequate qualitative results for the steady-state simulation of stirred tanks.

Computational Fluid Dynamics (CFD) software Fluent 6.3.26 was used to simulate flow in the real baffled tank of particular geometry. CFD simulation results are analyzed in terms of the predicted flow field, axial velocity component, turbulent kinetic energy and turbulent intensity and evaluated using the power obtained from experimental data. The general flow field and mean fluid velocity predictions were strongly influenced by either the turbulence model or the discretization scheme.

The results revealed a qualitative answer to the problem proposed as well as the path to improve the mixing quality in this particular stirred tank.

Keywords: Stirred, Tank, Power, CFD, Turbulence Model

Index

Nomenclature

$C_{\mu,s}$	Model parameters of the standard $\kappa - \varepsilon$ model	
$C_{1,s}$	Model parameters of the standard $\kappa - \varepsilon$ model	
$C_{2,s}$	Model parameters of the standard $\kappa - \varepsilon$ model	
D	impeller diameter	m
Fr	Froude number	
g	acceleration of gravity	m/s^2
H	liquid height in the tank	m
I_c	electric current	A
N	impeller rotational speed	rpm
P	power requirement of the impeller	W
P_k	production of turbulent energy kinetic	
Po	power number	
Re	Impeller Reynolds number	
W	Impeller width	m
u	mean velocity component	
u'	velocity fluctuation	
$\overline{u}$	mean flow velocity	
p	Power factor	
x	principal coordinate	

Greek symbols

δ	Kronecker delta	
κ	turbulent kinetic energy	m2/s2
ε	turbulent dissipation rate	m^2/s^3
ρ	fluid density	kg/m^3
σ	parameters in $\kappa - \varepsilon$ models	
μ	absolute viscosity	Poise
ν_{eff}	effective eddy viscosity = sum of laminar and turbulent eddy viscosity	
ν_{turb}	turbulent eddy viscosity	
ϕ	phase angle	

Subscripts

i, j	any principal direction
’	root mean square value

Abbreviations

ASM	Algebraic Stress Model
CFD	Computational Fluid Dynamics
IBC	Impeller Boundary Conditions
LDV	Laser Doppler velocimetry
MRF	Moving Reference Frame
QUICK	Quadratic Upwind Interpolation
UDF	User Defined Function

1 Introduction

1.1 Preface

Stirring is a method whereby mixing phases can be accomplished and by which mass and heat transfer can be enhanced between phases or external surfaces. This operation, which includes mixing as a special case, is well established in a wide variety of chemical processes.

Specifically, stirrers are applied to three general types of problems:

A. To produce static or dynamic uniformity in multicomponent multiphase systems,
B. To promote mass or energy transfer between the parts of a system not in equilibrium,
C. To promote phase changes in multicomponent system with or without a change in composition.

Stirred tanks are an important engineering area considering the number of processes, which are accomplished in tanks. Several physical or transport processes can occur during mixing in tanks.

Fluid mechanics and tank geometry are key points to understand mixing phenomenon. The fluid mechanics transports the material about the tank, whereas the geometry determines the fluid behavior. In fact, the geometry is so important that the processes can be specific for each type of geometry. Solid suspension is extremely dependent on the form of the tank bottom; liquid-liquid dispersion depend upon the geometry of the impeller; blending, upon the relative size of the tank to the impeller; and power draw is very much dependent upon the impeller geometry.

The mixing efficiency of a stirred tank is affected by at least the following parameters: baffles, tank geometry, impeller type, clearance, impeller speed, solubility of substance and eccentricity of the impeller.

A vortex is produced due to centrifugal force acting on the rotating liquid. If the vortex reaches the impeller severe air entrainment occurs. The depth and the shape of the vortex depend on impeller and vessel dimensions as well as on rotational speed. Normally this type of phenomena occurs on open top stirred tanks.

Flow patterns can be changed according to the type of impellers, and fall into three categories: axial, radial and tangential. The present work focuses on axial flow impellers.

Axial flow discharge coincides with the axis of impeller shaft, so when the impeller operates in a down pumping mode, the flow impinges on the bottom of the tank and spreads out in all directions toward the wall. The flow rises along the walls up the liquid surface and is pulled

back to the impeller. Since an axial flow impeller produce only one loop, fluids mix faster and blending time is reduced compared to radial flow impellers. The fluid does not take sharp turns near the impeller and because of this, power consumption is less than that of radial flow impellers at the same speed and same the diameter.

Consider a stirred tank with a Newtonian fluid of density ρ, and viscosity μ with an impeller of diameter D and rotating at rotational speed N. The tank diameter is T, the impeller width W and the liquid depth H. The power requirement of the impeller P represents the rate of energy dissipation within the liquid and depends on the following variables:

$$P = P\,(\rho, \mu, N, g, D, T, W, H,) \qquad 1.1$$

There is no functional relationship in equation 1.1 because of the complex geometry of the vessel, impeller and other inserts such as heating coils. Using dimensional analysis, the number of variables describing the problem can be minimized and equation 1 reduces to:

$$\frac{P}{\rho N^3 D^5} = function\,(\frac{\rho N D^2}{\mu}, \frac{N^2 D}{g}, \frac{T}{D}, \frac{W}{D}, \frac{H}{D}, etc) \qquad 1.2$$

where

$\frac{P}{\rho N^3 D^5}$ is the power number, Po

$\frac{\rho N D^2}{\mu}$ is the Reynolds number, Re

$\frac{N^2 D}{g}$ is the Froude number, Fr

Power consumption is associated with fluid viscosity, fluid density, rotational speed and impeller diameter.

This project had its origin on paint quality issues referenced by some of the most exigent customers of SunChemical Portugal. Preliminary studies conclude that the Titanium Dioxide (TiO2) was not sufficiently dispersed on the continuous phase of the paint by the available stirred tank. As a result, the paint production had to be dislocated to the SunChemical facilities in Spain, where the respective stirred tank had a higher power rotor and could assure the high quality standard inherent to SunChemical paints. Thus, enhancing the mixing quality of the “Portuguese” stirred tank is urgent. To do so, an attempt to introduce a second impeller on the stirred tank was made keeping the same rotor.

This work presents the results of the first studies done on this project and their practical effect on the SunChemical process.

1.2 Aim of this contribution

The aim of this work is to investigate the effects of the implementation of a new impeller on the CFD simulation of fluid flow in a stirred tank using the MRF impeller rotation model and the $\kappa - \varepsilon$ turbulence model. In particular, this work aims to study the effect of a second impeller on the enhancement of the solid/liquid mixture in an industrial stirred tank by analyzing the flow patterns and their effect on the power consumption. Due to its particular impeller and tank geometries, the available time dedicated to this project and tools available, this study must be considered as a first attempt to describe this particular stirred tank.

1.3 Contents

The information available on this project is organized to facilitate the understanding of the path followed to relate the tank geometry and operation with simulation models used to calculate the dissipated power.

This chapter provides a brief introduction to the project research area and contents which are going to be explained in detail in subsequent chapters. The main objectives are also stated as, the contextualization with the problem attached to the stirred tank study. The purpose is not on making a complete review but on providing the basic information to understand the inherent complex flow.

Chapter 2, State of the Art, gives a view on the CFD potential for stirred tank hydrodynamics stating the governing equations behind the flow and turbulence modeling. The considerable effects of the grid and discretization scheme on the final results are also stated as well as the challenging choice of turbulence models.

Chapter 3, Results and Discussion, clarifies the initial data provided and its adaptation to workable values. Here it is provided a necessary view on the stirred tank geometry, acknowledging their implications and particularities, establishing a basis for the hydrodynamic patterns and predicted power results. The results are divided into two main cases: *Liquid* and *Base*. According to each case, the explanation for the simulation results are stated and compared with the proposed impeller configuration.

The main conclusions found from this thesis are presented in Chapter 4.

One of the most important parts of this report is stated in Chapter 5, Evaluation, where the objectives accomplished are mentioned along with the some important limitations and/or difficulties inherent to this project. The author personal evaluation is also reported in this chapter.

The results discussed in Chapter 3 have their origin on previous case studies linking the effect of CFD statement with the tanks power consumption. The most relevant case studies are summarized in Chapter 7, Appendices.

2 State of the art

Stirred tank is a type of equipments widely used in chemical, pharmaceutical, metallurgical and wastewater process industries. They are mainly used for mixing different phases (liquid-liquid, solid-liquid, gas-liquid, solid-liquid-gas, etc), but also to perform chemical reactions, precipitation processes and crystallizations.

This class of process equipments has been extensively studied throughout the years. However, due to the diversity of tank geometries, impellers and phase systems, the transferability of the modeling knowledge from one stirred tank to another is very difficult to achieve.

Stirred tanks offer unmatched flexibility and control over transport processes occurring within the tank. Parameters such as tank shape, aspect ratio, number, type, location and size of impellers and degree of baffling provide effective handles to control the performance of stirred tanks. However, the availability of such a large number of parameters also makes the job of selecting the most suitable configuration for the stirred tank quite difficult. Once the desired flow characteristics are identified, it is then necessary to use or to develop appropriate tools to relate tank hardware and operating conditions to resulting flow within the tank.

CFD provides a tool for studying the hydrodynamics of the process which can be the basis to diagnose and model a stirred tank (T. Kumaresan, 2006). There are four main aspects to consider before make full use of the CFD capabilities (D.A. Deglon, 2006): grid resolution, discretization scheme, turbulence model and impeller rotation model.

The grid resolution is clearly important in any CFD simulation. Usually it is necessary to carry out simulations until no enhancement on the final solution is achieved. Some authors focused their study on small grids in partial stirred tank geometries, trying to output the effect of the increase of the grid resolution (Ng, 1998). It was shown that successively finer grids yielded equivalent predictions of mean velocity profiles which were in good agreement with experimental LDV data but that the turbulent kinetic energy was severely under-predicted on all grids, with the finer grids showing only marginal improvement. Thus, these authors conclude that further grid refinement was unlikely to result in better predictions. Nevertheless, the level of successive grid refinements mentioned in these, and other studies, was relatively small and may not display accurate grid dependency of the turbulent kinetic energy. For example, the studies of Wechler (1999), which involved grid sensitivity studies of up to over a million control volumes, proved that extremely fine grids are required to isolate numerical and model errors in the prediction of turbulence quantities.

The transport equations describing the instantaneous behavior of turbulent liquid flow are the three Navier - Stokes equations (transport of momentum in the three spatial coordinates *r*, *z*, φ for a cylindrical polar coordinate system) and a continuity equation. The instantaneous velocity components and the pressure can be replaced by the sum of a time-averaged mean component and a root-mean-square fluctuation component according to Reynolds. The resulting Reynolds-averaged Navier-Stokes equations and the continuity equation are summarized below:

$$\frac{\partial(\rho u_i)}{\partial t} + \frac{\partial(\rho u_j u_i)}{\partial x_j} = -\frac{\partial}{\partial x_i}\left(\tau_{ij} + \rho u_i' u_j'\right) - \frac{\partial p}{\partial x_i} + \rho g_i \qquad 2.1$$

$$\frac{\partial \rho}{\partial t} + \frac{\partial}{\partial x_i}(\rho u_i) = 0 \qquad 2.2$$

where

The Reynolds stresses (see Eq. (2.1) : $\rho u_i' u_j'$) are described by Reynolds stress models or eddy viscosity models. A Reynolds stress model consists of six transport equations for the individual Reynolds stresses and one transport equation for the energy dissipation rate ε; in total: seven transport equations related only to turbulence modeling. Although implemented in several commercial CFD software packages the solution of these seven complex equations, together with the three Reynolds equations and the continuity equation, is not a trivial task and it is computationally expensive.

Approximations to the Reynolds stress models, called algebraic stress models, adapt the partial differential equations of the individual Reynolds stresses into algebraic equations. Solutions are then required for these algebraic equations and the two partial differential equations for the turbulent kinetic energy κ and the energy dissipation rate ε. (Bakker, 1994) followed this approach of turbulence modeling. A reasonable compromise for model accuracy and computational expense are eddy viscosity models' relating the individual Reynolds stresses to mean flow gradients:

$$\rho u_i' u_j' = -\rho \nu_{turb}\left(\frac{\partial u_i}{\partial x_j} + \frac{\partial u_j}{\partial x_{ji}}\right) + \frac{2}{3}\rho \delta_{ij} \kappa \qquad 2.3$$

where ν_{turb} is the turbulent eddy viscosity. The transport of momentum, which is related to turbulence, is thought of as turbulent eddies, which, like molecules, collide and exchange momentum. The family of two-equation $\kappa - \varepsilon$ models is the most widely used of the eddy

viscosity models. A $\kappa - \varepsilon$ model consists of two transport equations, one for the turbulent kinetic energy κ and one for the energy dissipation rate ε. Only two instead of seven transport equations are used to describe the main characteristics of turbulence: production, dissipation, convective and dissipative transport. The turbulent eddy viscosity is calculated from

$$\nu_{turb} = c_\mu \frac{\kappa^2}{\varepsilon} \tag{2.4}$$

where c_μ is a parameter, which depends on the specific $\kappa - \varepsilon$ model.

The standard $\kappa - \varepsilon$ model, as presented by (Launder, 1972), is most widely used two-equation eddy viscosity model, also for modeling turbulence in stirred-tank reactors. The attractiveness of this model and its wide use and testing, has thrown light on both its capabilities and its shortcomings, which are well-documented in the literature (Launder, Prediction of free shear flows - a comparison of the performance of six turbulence models, 1972);(Kim, 1978);(Pope, 1978);(Hanjalic, 1980);(Kline, 1981); (Roback, 1983). For high turbulent Reynolds numbers, the model may be summarized as follows:

$$\frac{\partial(\rho k)}{\partial t} + \frac{\partial}{\partial x_i}(\rho u_i k) = \frac{\partial}{\partial x_i}\left(\rho \frac{\nu_{eff}}{\sigma_{k,S}} \frac{\partial k}{\partial x_i}\right) + \rho(P_k - \varepsilon) \tag{2.5}$$

$$\frac{\partial(\rho \varepsilon)}{\partial t} + \frac{\partial}{\partial x_i}(\rho u_i \varepsilon) = \frac{\partial}{\partial x_i}\left(\rho \frac{\nu_{eff}}{\sigma_{\varepsilon,S}} \frac{\partial \varepsilon}{\partial x_i}\right) + \rho\left(C_{1,S}\frac{\varepsilon}{k}P_k - C_{2,S}\frac{\varepsilon}{k}\varepsilon\right). \tag{2.6}$$

The production of turbulent kinetic energy P_k is modeled with the aid of the eddy viscosity hypothesis:

$$P_k = \nu_{turb}\left(\frac{\partial u_i}{\partial x_j} + \frac{\partial u_j}{\partial x_i}\right)\frac{\partial u_j}{\partial x_i} \tag{2.7}$$

The dissipation rate ε can be regarded as the rate, at which energy is being transferred across the energy spectrum from large to small eddies. The standard $\kappa - \varepsilon$ model assumes spectral equilibrium, which implies that, once turbulent kinetic energy is generated at the low-wave number end of the spectrum (large eddies), it is dissipated immediately at the same location at the high-wave-number end (small eddies). In other words, the standard $\kappa - \varepsilon$ model assumes that P_k is near to ε. As far as the stirred vessel is concerned, this is a very restrictive assumption, because there is a vast size disparity between those eddies, in which turbulence

production takes place (mainly at the stirrer), and the eddies, in which turbulence dissipation occurs.

Since CFD is based on the Navier–Stokes equations and mathematical models, simplifying some assumptions will generate some discrepancies. Among these are the type of modeling approach employed, i.e. impeller boundary conditions (IBC), steady state or transient models, turbulence models and discretization schemes.

Several studies have focused on the effect of various turbulence models on the final numerical solution. Most commonly, a comparison between the standard $\kappa - \varepsilon$ and RNG $\kappa - \varepsilon$ models has been made. (Z. Jaworski K. D., 1997) studied the flow produced by a Rushton turbine using a sliding mesh and reported that the type of turbulence model did not have much effect on the mean velocities. But in the majority of these studies, poor prediction of turbulence quantities has been attributed to deficiencies in this model, especially the inherent assumption of isotropic turbulence and limitations in predicting swirling or recirculating flow (**Abujelala and Lilley, 1984; Armentante et al., 1997; Jenne and Reuss, 1999**). Several authors have compared flow predictions in stirred tanks using variations of the $\kappa - \varepsilon$ model such as the Chen - Kim and Renormalized Group (RNG) $\kappa - \varepsilon$ models **(Ranade et al., 1989; Jenne and Reuss, 1999; Jaworski and Zakrzewska, 2002; Aubin et al., 2004)**. Generally, the different variations have resulted in only slight changes in turbulence predictions, and in some cases the standard model gave superior results. It has been suggested that a turbulence model that is not based on the assumption of isotropic turbulence should give better results. **Armentante et al. (1997)** found that the Algebraic Stress Model, ASM, gave superior results that the standard $\kappa - \varepsilon$ turbulence model. However, in some published studies the Reynolds Stress Model based on non-isotropic turbulence was found to yield turbulent kinetic energy profiles showing a larger deviation from experimental values than those obtained using the standard $\kappa - \varepsilon$ model **(Montante et al., 2001; Jaworski and Zakrzewska, 2002)**.

The use of large eddy simulation for modeling flow in stirred tanks has been reported to result in good agreement with experimental data for both mean velocities and turbulence quantities **(Eggels, 1996; Derksen and Van Den Akker, 1999; Hartmann et al., 2004)**. However, due to limitations on grid requirements and the associated computational expense, LES techniques are impractical for many research problems, including this one.

The discretization scheme effect was studied by some authors including **(Aubin J., 2004)**. This author covered three schemes: first order upwind, upwind-central hybrid and QUICK. The results showed that the discretization scheme had little or no effect on the mean velocities and all three under-predicted the turbulent kinetic energy. The quality of the mixing can be

assured by analyzing the relative distribution of the mean and turbulent kinetic energy **(D.A. Deglon, 2006)**.

These results showed good agreement with experimental results except for the trailing vortex region. The turbulence quantities were found to be largely under-predicted, although better agreement with experimental data was found for the standard $\kappa - \varepsilon$ model than the RNG $\kappa - \varepsilon$ model. Later (Z. Jaworski W. B.) reported similar results to those previously discussed but for a dual Rushton turbine geometry with a tracer simulation.

Without the tracer, similar results were found to those by (Z. Jaworski K. D., 1997), with the tracer however, solution stability problems were experienced with the RNG $\kappa - \varepsilon$ model and the flow could not be computed.

The MRF technique (J.Y. Luo, 1995) is a steady state approximation for problems where the distance between the impeller blades and baffles is sufficient such that the flow in the vicinity of the impeller is unaffected by the rest of the tank and can be assumed to be time independent with respect to the impeller. The resulting flow field is representative of a snapshot of the transient flow field in which the rotation parts are moving. Thus if an interface can be drawn on which there is little or no angular dependence, the model can be a reliable tool for simulating time-average flow fields. (D.A. Deglon, 2006) experiments have shown that the region where flow is strongly influenced by the periodic passage of the blades extends to a radius of D/2 away from the impeller tip and 1.5 blade heights above and below the impeller disk.

3 Results and Discussion

The stirred tank studied here works in batch mode performing solid/liquid mixing for paint production. The continuous phase is a solvent *CV1221009*. The solvent is the liquid in paint that suspends the pigment and/or resins and transports them from the paintbrush to the wall. Solvents in paint can be water (for latex paint) or mineral spirits (for oil based alkyd paint).

The dispersed phase is titanium dioxide (TiO_2). When used as a pigment, it is called *titanium white* or *pigment white 6*. Due to its brightness and very high refractive index ($n = 2.7$) it is considered the most widely used white pigment. The objective of this process is to uniformly distribute the dispersed phase within the continuous phase.

3.1 Initial Data

The total mass to be mixed has a value around 2700 kg from which 1000 kg are TiO_2, approximately 37 %. The operation procedure is show in Table 3.1.

Table 3.1 - Operation procedure and parameters measured.

Time [min]	I_c *[A]*	*T (ºC)*	*Comments*
0	95	15	
1	96	15	
3	98	15	Begin TiO_2 addition
4	104	15	
7	110	16	
9	117	17	
15	117	21	
25	114	29	End TiO_2 addition
30	113	30	

The total stirring time is 30 minutes or 21 minutes considering only the time after complete TiO_2 addition. The electric current, I_c, consumed by the stirred tank rotor is also shown in Table 3.1. In order to have an experimental value of the dissipated power to the mixture, it was assumed that the rotor has the following characteristics listed in Table 3.2 where U_c is the ratio of the real power to the apparent power and $\cos(\phi)$ refers to the angle by which the peak voltage leads or lags the current.

Table 3.1– Rotor power characteristics assumed.

Power Characteristics	
$\boldsymbol{U_c}$ **[V]**	400
$\mathbf{cos}\ (\boldsymbol{\phi})$	0.85

The experimental of powers for each electric current measured is given by

$$P = \sqrt{3} \times Uc \times I \times \cos\ (\phi) \times 0.001 \qquad 3.1$$

The experimental values powers as a function of the electric current were provided by SunChemical and are shown in Table 3.3.

Table 3.3 – Experimental powers results based on the electric current measured.

I *[A]*	$\boldsymbol{P}$ *[kW]*
95	43.4
96	43.9
98	44.8
104	47.6
110	50.3
117	53.5
117	53.5
114	52.1
113	51.7

The maximum power possible to dissipate to the mixture is given by the design value and it corresponds to $\overline{P_{SunChemical}} = 55\ kW$. Thus if an additional impeller is adapted to this tank geometry, its effect on the dissipated power should not increase more than 1.5 kW or 2.7% of the actual power.

The load properties used on the Liquid and Base simulations are listed in Table 3.4.

Table 3.4 - Load main properties.

Load	***ρ [kg/m3]***	***μ [Poise]***	***N [rpm]***
Liquid	1260	0.946	1460
Base	1350	17	1460

Finally the stirred tank operates at 1460 rpm. This is the impeller design value, and no measurements were made to determine the real rotation speed, but it was assured from Sunchemical that the value is correct.

3.2 Geometric Model

The stirred tank geometric model was built in ANSYS software GAMBIT 2.3.16. Due to the computational capability it was feasible to simulate the entire stirred tank using about 1.8 million volume elements. The photos and dimensions were provided by SunChemical as shown in Fig 3.1 and 3.2.

Fig. 3.1 - Stirred tank at SunChemical.

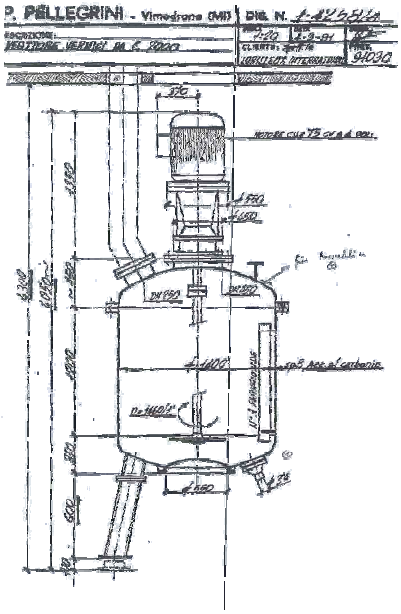

Fig. 3.2 - Stirred tank dimensions.

The stirred tank studied is a vessel of 1.4m diameter with three baffles. The 0.070m diameter top shaft is positioned in the center of the stirred tank. Fig. 3.3 shows an axial slice of the stirred tank, where it is possible to visualize its interior details.

This particular stirred tank has uncommon characteristics when comparing with the usual stirred tank. It is hard to find stirred tanks with only three baffles. Due to all this characteristics the transferability of power data between this work and the publications found on the references was virtually none. The impeller geometry was built following the indications on the impeller design (Fig. 3.4). As shown in Fig. 3.5 the impeller has a unique sharp geometry designed to *cut out* the solvent as well as to attempt to create big large vortices inside the tank.

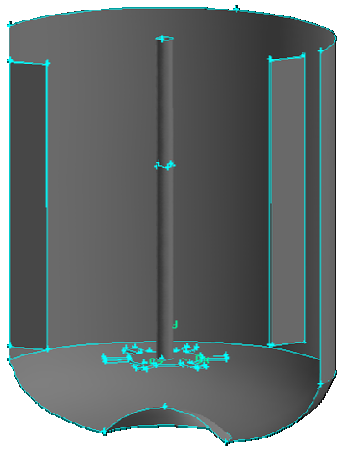

Fig. 3.3 – Axial cut of stirred tank, showing lower impeller.

It consists on a disc with six blades equally spaced, similar to a Rushton impeller(K.H. Javed, 2006), but the blades are as thin as the disk and with an inclination angle of approximately 30 degrees.

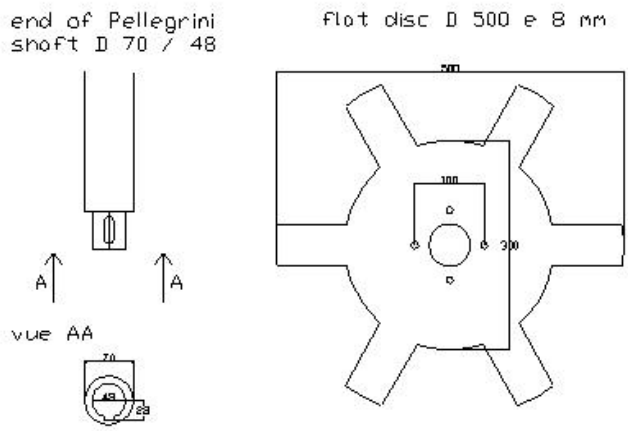

Fig. 3.4 - Stirred tank lower impeller dimensions.

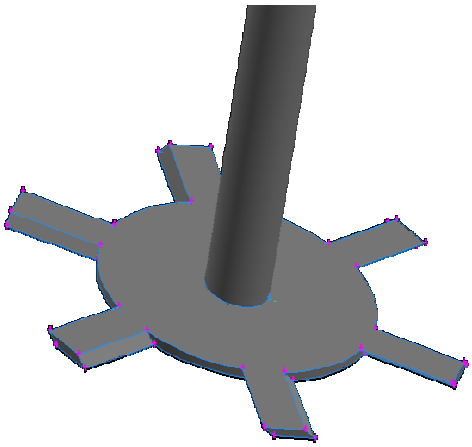

Fig. 3.5 - Stirred tank lower impeller.

As previously mentioned, for the second phase of this work it was needed to create a second impeller geometry. Fig. 3.6 shows zoom of the axis of the stirred tank, where it is possible to visualize the upper impeller composed by four blades 1 mm thin and 19º of inclination on the lateral faces. The dimensions were empirically imposed as well as the location. The type of impeller was selected based on the available impellers and easiness of application. This is a

traditional impeller for large volume applications where a degree of fluid shear is beneficial to the overall process result.

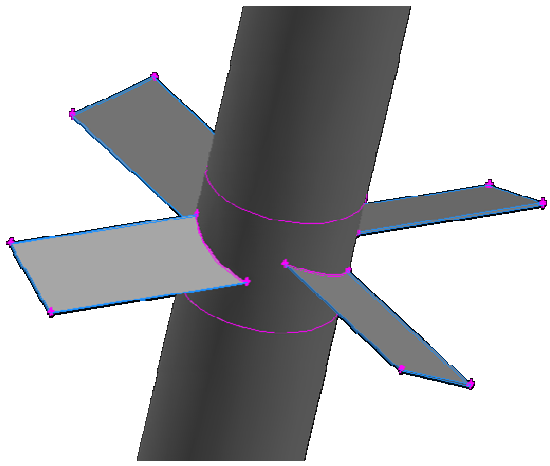

Fig. 3.6 - Upper impeller configuration.

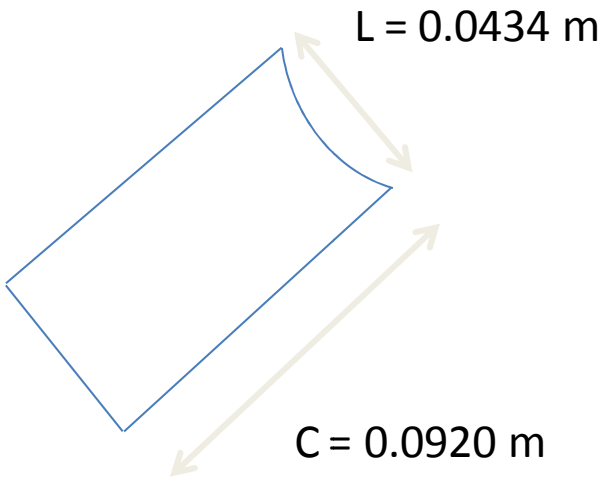

Fig. 3.7 - Upper impeller dimensions.

The geometric model with both lower and upper impeller is shown on Fig 3.8.

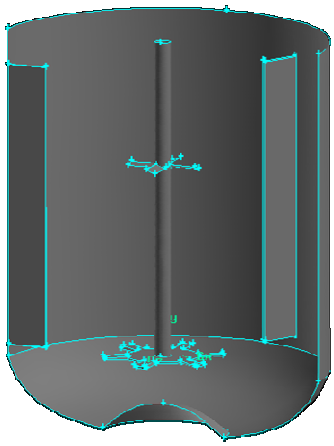

Fig. 3.8 – Axial cut of stirred tank, showing second impeller.

3.3 3D Simulations

The stirred tank simulation model was built in ANSYS software FLUENT 6.3.26. Due to the available computational capabilities it was feasible to simulate the entire stirred tank by

dividing it into four processement zones. A single processor was attributed to each zone to improve the computational time and consequently the number of simulations performed.

In this project, the simulation model should be able to predict the power requirements as well as the hydrodynamics of flow inside the stirred tank. Therefore it was necessary to conduct several simulations to enhance the power results and to understand the effects of the given variables on the process. In a following section are presented the cases studies performed to analyze the best suitable models plus the effects of the rotational speed and viscosity on the dissipated power, after some prior considerations that must be stated.

As previously mentioned, MRF was the rotational model chosen to simulate the stirring. To use this model it is essential to indicate both the rotational direction and the rotational speed. The rotational direction chosen was clock-wise in all cases, so that the impeller blades induce a downward flow in the bottom center of the tank.

After tuning up the simulation parameters two main simulations were performed for each load; one for each impeller configuration.

The two main loads consider for this work are designated by Liquid and Base. Liquid is the designation given to a fluid containing various pigments and/or dyes. Base is the designation given to the Liquid after the TiO_2 addiction. The predicted results are stated in the following sections.

3.3.1 Liquid

3.3.1.1 Streamtraces

A streamtrace is a path traced by a massless particle placed at and arbitrary location in a steady-state vector field. A streamtrace can be colored to represent a given flow variable, being the color range proportional to the variable's magnitude. Streamtraces therefore have the ability to convey not only the relative movement of the flow, but the relative speed as well. In the present work, a set of streamtraces suitably located can provide both qualitative and quantitative information about the hydrodynamics of the stirred tank.

To compare different configurations, the streamtraces were placed in the same location and in the same number. Figure 3.9 represents the streamtraces for both configurations, colored with velocity magnitude. It is possible to identify the main paths by which the fluid elements pass. Apparently the differences between the flow patterns are not very significant. Nevertheless, for the alternative configuration, the flow between both impellers is more obvious than in the default configuration. The flow rises along the walls up the liquid surface and is pulled back to the impeller.

(a)

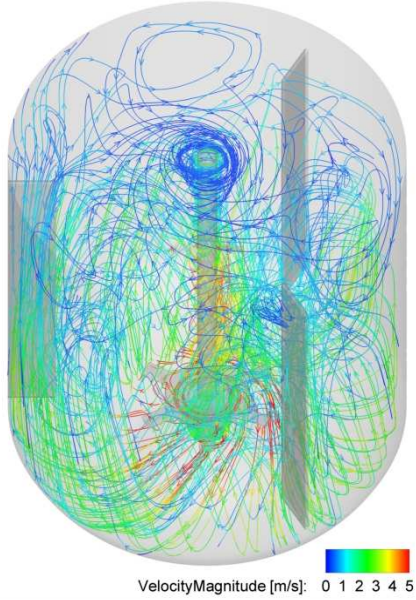

(b)

Fig. 3.9 - Velocity magnitude streamtraces: a) Lower impeller configuration; b) Upper and lower impeller configuration.

Since the axial flow impeller produces only one loop, fluids mix faster and the mixing time is reduced compared to radial flow impellers. This is the basic principle behind this kind of stirred tanks and it is notorious on both Fig. 3.10.

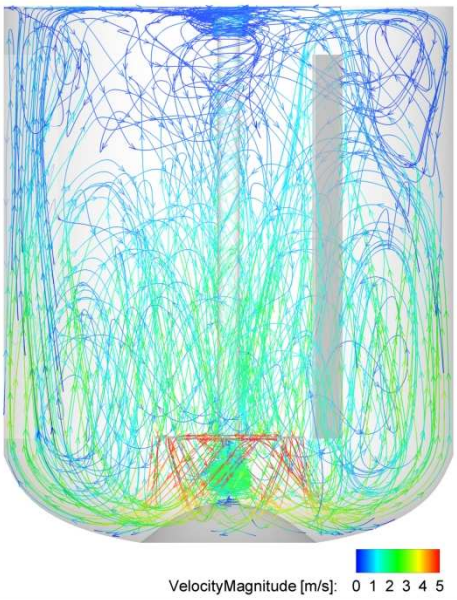

(a)

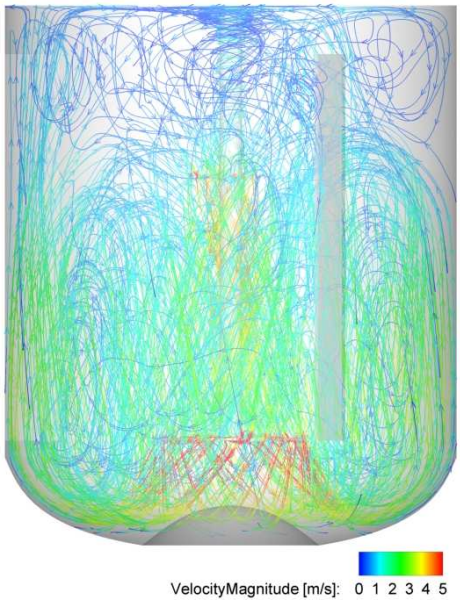

(b)

Fig. 3.10 - Velocity magnitude streamtraces: a) Lower impeller configuration; b) Upper and lower impeller configuration.

At the top of the stirred tank the streamtraces show a zone with flow patterns of smaller velocities. With the upper impeller configuration the axial flow pattern (along the wall) is more notorious than with only the lower impeller, reducing the volume of lower velocity fluid situated at the top of the tank. Assuming that the volume at the top of the tank is not in a closed loop, the upper impeller configuration slightly improves this zone turbulence.

3.3.1.2 Axial Velocity

Another way to understand the complex flow patterns inside the stirred tank is through the velocity axial component. This component shows the contribution to the fluid to flow up, along the wall of the stirred tank. By analyzing Fig. 3.11 is it clear that the upper configuration enhances the loop by impelling the fluid down near zone at the top of the tank.

At this point some words should be said about the effect of the baffles. Baffles are flat vertical strips set radially along the tank wall. Baffles reduce the tendency of the fluid to have only rotational movement, a situation that does not promote mixing. In baffled tanks, a better concentration distribution throughout the tank and consequently improvement in the mixing efficiency is achieved.

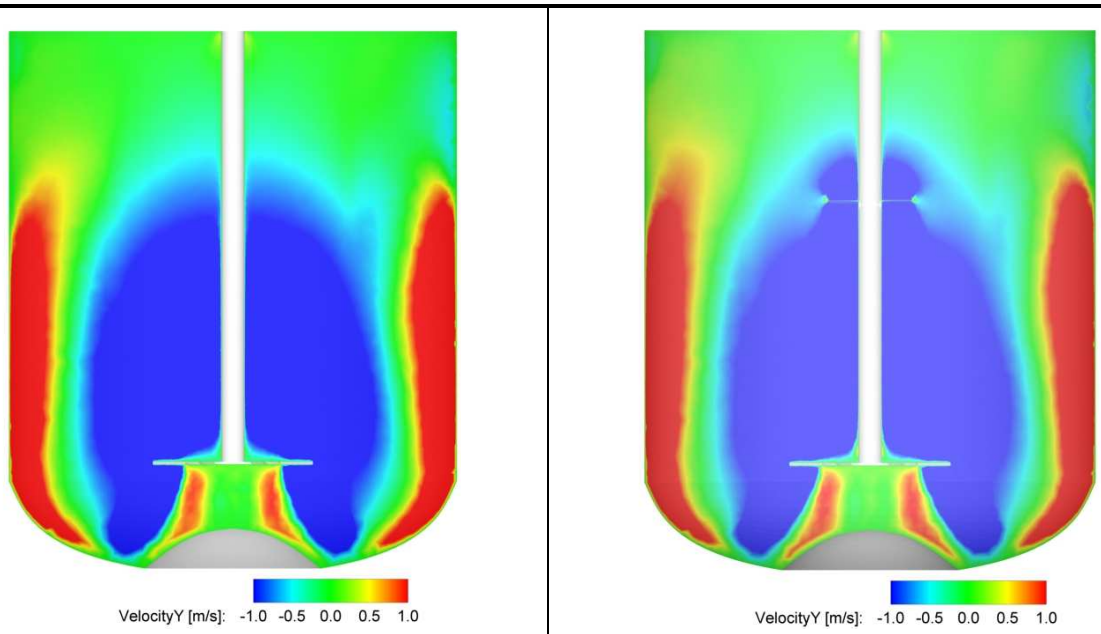

(a)	(b)

Fig. 3.11 - Axial velocity, axial slice: a) Lower impeller configuration; b) Upper and lower impeller configuration.

The larger the width of the baffles, the better is the mixing to some extent. As shown in the Fig. 3.12, the three baffles avoid solid block rotation by splitting the main loop.

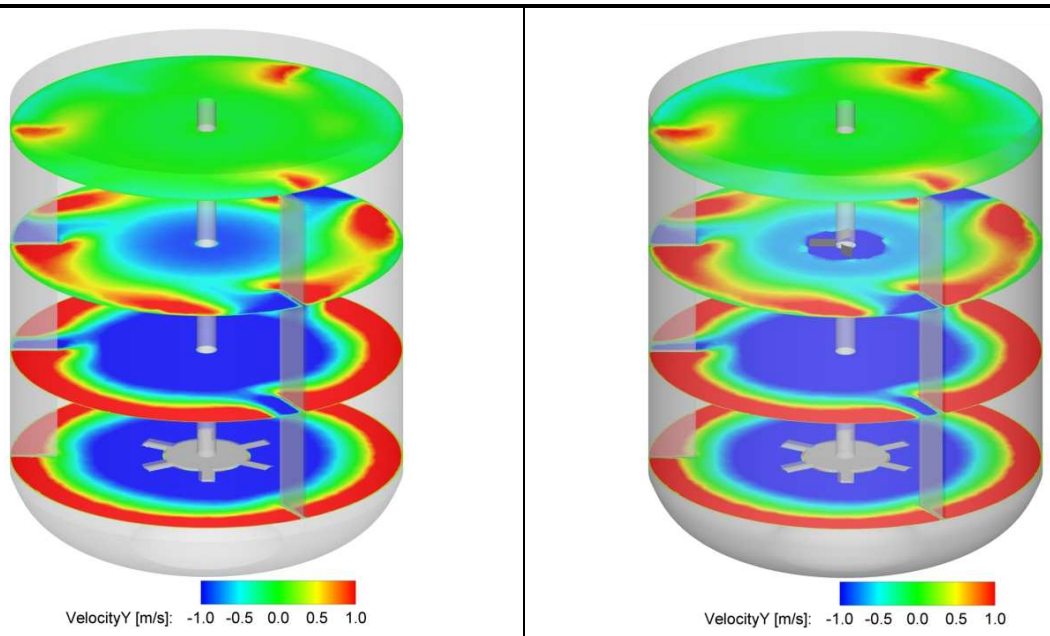

(a)	(b)

Fig. 3.12 - Axial velocity, represented at slices at different axial positions: a) Lower impeller configuration; b) Upper and lower impeller configuration.

Consider the space between two baffles along the tank wall. As previously said, the impeller rotation is clock-wise. So at the front of the first baffle the fluid velocity is increasingly more positive as we get close to the tank. On the other hand at the back of the second baffle the fluid velocity is increasingly more negative as we approach the tank top. Is clear on the upper impeller configuration that in the upper slice, the velocity magnitudes are higher and thereby the mixing loop embraces more fluid.

3.3.1.3 Turbulent Kinetic Energy

Turbulent kinetic energy measures the turbulent effect on the fluid velocity. It is transferred to the fluid in progressively smaller scales. The predicted turbulent kinetic energy contours are shown for both impeller configurations on Fig. 3.13. It is clear from the figure that the upper impeller increases the turbulent kinetic energy in the upper region of the tank. In fact only near the upper and lower impellers, the fluid receives important kinetic contributions from the impeller. This indicates that the upper impeller is promoting mixing.

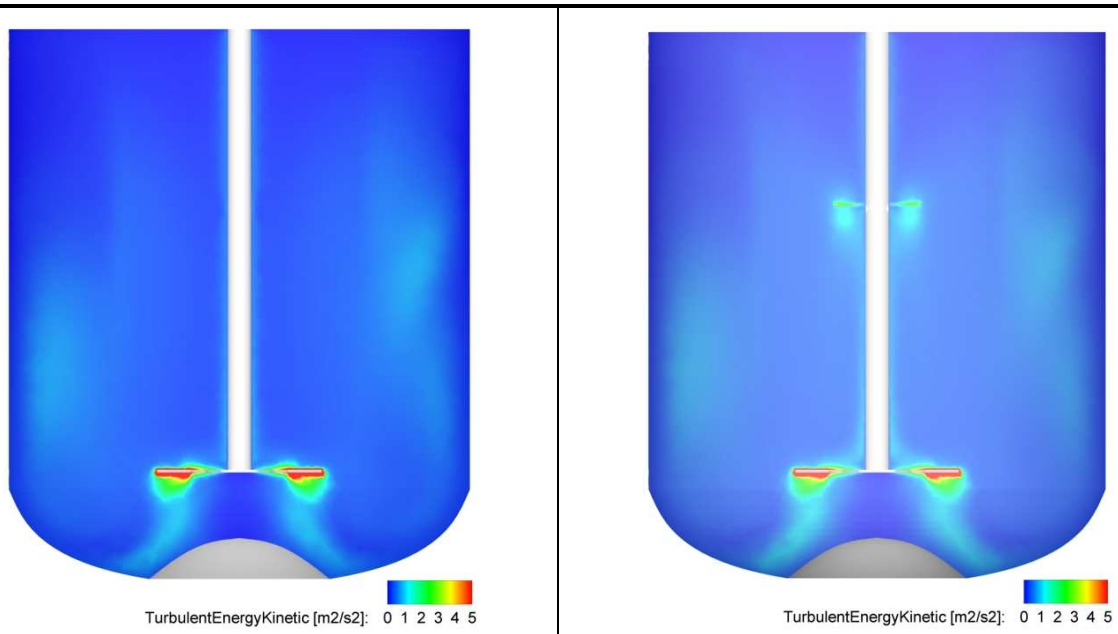

(a)	(b)

Fig. 3.13 - Turbulent Kinetic Energy, axial slice: a) Lower impeller configuration; b) Upper and lower impeller configuration.

The turbulent kinetic energy effect along the tank's height is shown on Fig. 3.14. The observations made for the axial slice can be applied on the analysis of these figures.

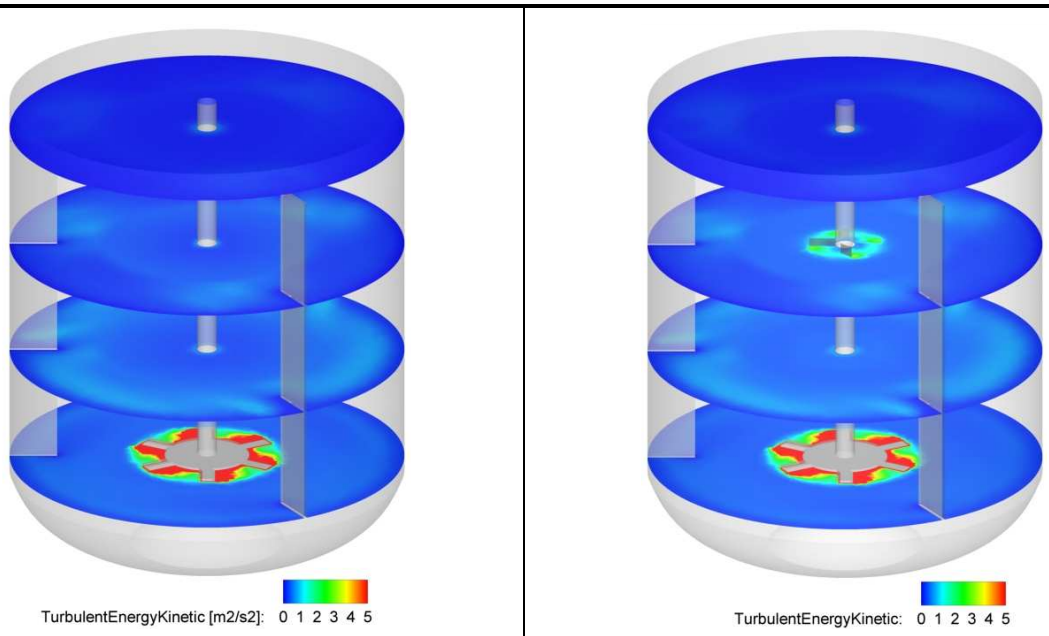

(a)	(b)

Fig. 3.14 - Turbulent Kinetic Energy, represented at slices at different axial positions: a) Lower impeller configuration; b) Upper and lower impeller configuration.

The upper impeller has a small effect along the tank, but it is clear the increase of the turbulent kinetic energy in the upper region. Again only near both impellers this effect is felt. If the quality of the mixing can be assured by analyzing the relative distribution of the turbulent kinetic energy **(D.A. Deglon, 2006)** than the upper impeller effect is clearly benefic to the overall mixing process.

3.3.1.4 Turbulent Intensity

The turbulent intensity, I, is defined as the ratio of the root-mean-square of the velocity fluctuations, u', to the mean flow velocity, $\overline{u}$. A turbulence intensity of 1% or less is generally considered low and turbulence intensities greater than 10% are considered high. In a stirred tank, its value can represent the level of turbulence suffered by the fluid.

Fig. 3.15 shows the effect of the both impeller configurations. For the lower impeller the turbulent intensities are practically uniform along the tank. As expected, near the lower impeller the fluid experiences turbulences intensities above 1 %. Although it was not the objective of this study, some research should be made in order to assess the vortices created near the blades of both impellers and their effect on the blade design and torque measurements. Near the upper impeller the turbulent intensity magnitude is not so high, but it is clear the increase in turbulent intensity around the impeller blades.

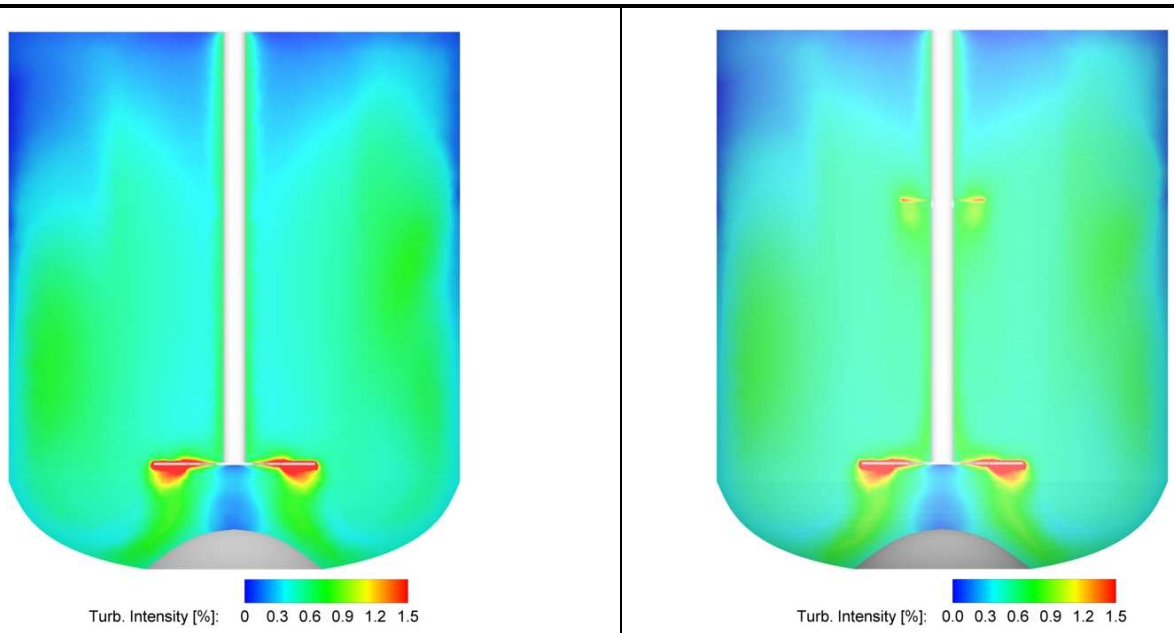

(a)	(b)

Fig. 3.15 - Turbulent Intensity, axial slice: a) Lower impeller configuration; b) Upper and lower impeller configuration.

Figure 3.16 intend to compare the differences between both impeller configurations along the stirred tank. At this point it should be noticed that the upper impeller geometry is originally designed for low viscosities loads promoting the fluid velocity instead of promoting high shear stresses.

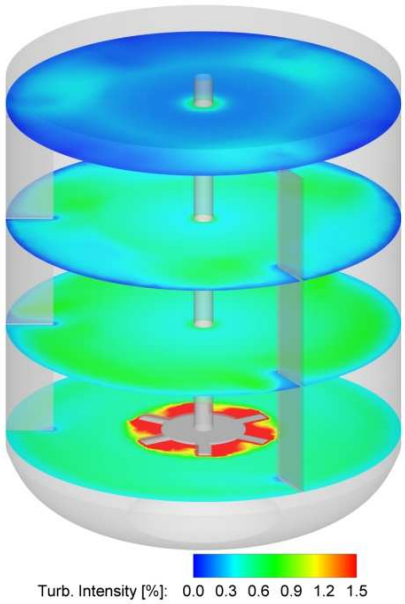

(a)

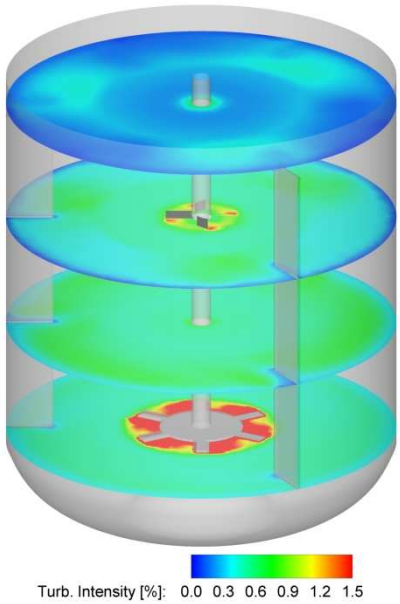

(b)

Fig. 3.16 - Turbulent Intensity, represented at slices at different axial positions: a) Lower impeller configuration; b) Upper and lower impeller configuration.

Thus, only a slight increase in turbulent intensity was achieved by the introduction of the upper impeller and consequently, assuming that the increase of the turbulent intensity is proportional to the increase of the mixing quality, a slight improve in mixing quality should be expected. It should be noticed that the motor power was already very close to the limit so the increase due to the extra impeller should be very small.

3.3.1.5 Power

The predictions of the power needed for both impeller configurations are shown on Table 3. 10. For the lower impeller configuration the power predicted was P_{FLUENT} = 58.6 kW, 6.5 % more power than the maximum power achieved by the stirred tank rotor.

Table 3.9 indicates that for the lower impeller the power predicted by CFD simulations is higher than the nominal power of the motor. This indicates that the model over predicts the

real power needed to this process, due to several possible reasons that will be explained later. Nevertheless, a comparison can be made in terms of relative variation.

Table 3.9 - FLUENT predicted results for the two impeller configurations.

ρ [kg/m^3]	μ [$Poise$]	N [rpm]	Impeller Configuration	M_{imp} [N.m]	P_{FLUENT} [kW]	P_{SunChe} [kW]	Impeller power effect
1260	0.946	1460	lower impeller	383.0	58.6 (+ 6.5%)	55	-
1260	0.946	1460	lower and upper impeller	459.5	70.3 (+ 27.8%)	55	+ 20.0%

For the lower and upper impeller configuration the power predicted was P_{FLUENT} = 70.3 kW, 27.8 % more power than the maximum power achieved by the stirred tank rotor.

Even though the case studies performed indicated that these results were possible, variations of such magnitude especially on the lower and upper configuration are unfeasible. As discussed in Section 3.1, the power available to input is 1.5 kW. Therefore the increase of 15.3 kW is as impractical as unrealistic.

A case study (Appendices – Case #1) was made approaching the effect of the rotational speed on the power prediction. The effect was notorious although the fluid viscosity was 25 Poise.

There are some aspects responsible for these results; this model assumes the fluid as isotropic meaning that its properties are identical in all directions. However the fluid property with a flagrant anisotropic effect is viscosity. In reality, the fluid is non-newtonian and consequently near the impeller, where the shear rates are higher, the fluid viscosity is lower, so assuming a constant viscosity, there is an over estimation of the shear stresses in the impeller and consequently on the power estimation.

3.3.2 Base

3.3.2.1 Streamtraces

Again, to compare both configurations, the streamtraces were placed in the same location and in the same number. Figure 3.17 represents the streamtraces for both configurations,

colored with velocity magnitude. These streamtraces are similar to the one displayed in Section 3.3.1.

As expected the domain near the upper impeller has larger velocities and the main loop along the tank reaches higher zones. It should be noticed that at the top of the tank, around the shaft, there is a recirculation volume or a vortex.

It is a relatively small vortice and with no important effect on the flow patterns inside the stirred tank. In practice, this vortice should create a depression in the gas-liquid surface, which would only be visible if a multiphase model was used. In the present studies, a fixed horizontal surface was used with full slip condition in order to simulate the gas-liquid interface.

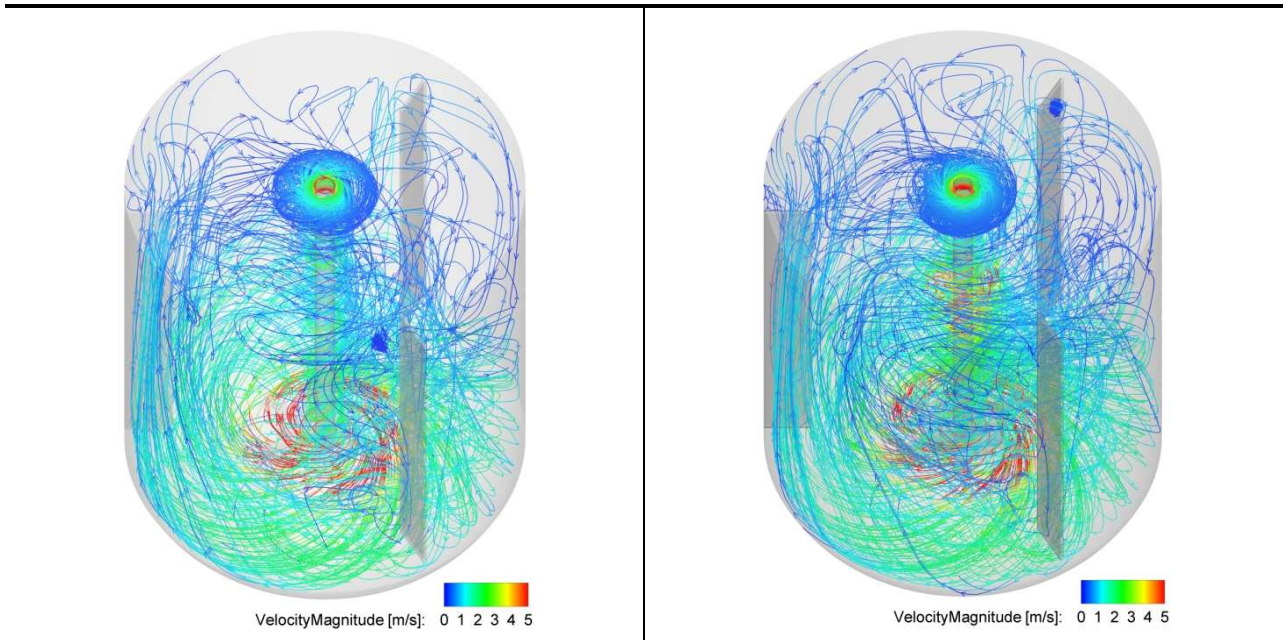

(a)	(b)

Fig. 3.17 - Velocity magnitude streamtraces: a) Lower impeller configuration; b) Upper and lower impeller configuration.

Figure 3.18 allow a better understanding of the fluids loop along the tank. In theory, only one major loop should appear on the tank due the type of lower impeller. The upper configuration provides a benefic radial flow near the top of the tank, enhancing the mixing quality in a hard agitation section of the stirred tank.

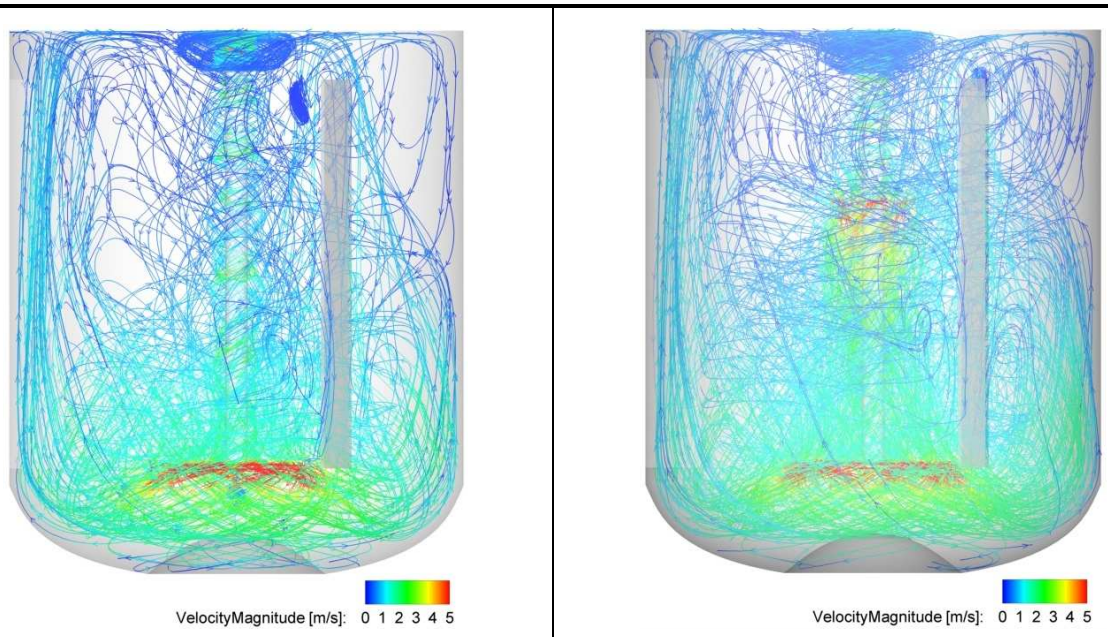

(a) (b)

Fig. 3.18 - Velocity magnitude streamtraces: a) Lower impeller configuration; b) Upper and lower impeller configuration.

3.3.2.2 Axial Velocity

Figure 3.19 shows the axial velocity contours for both impeller configurations.

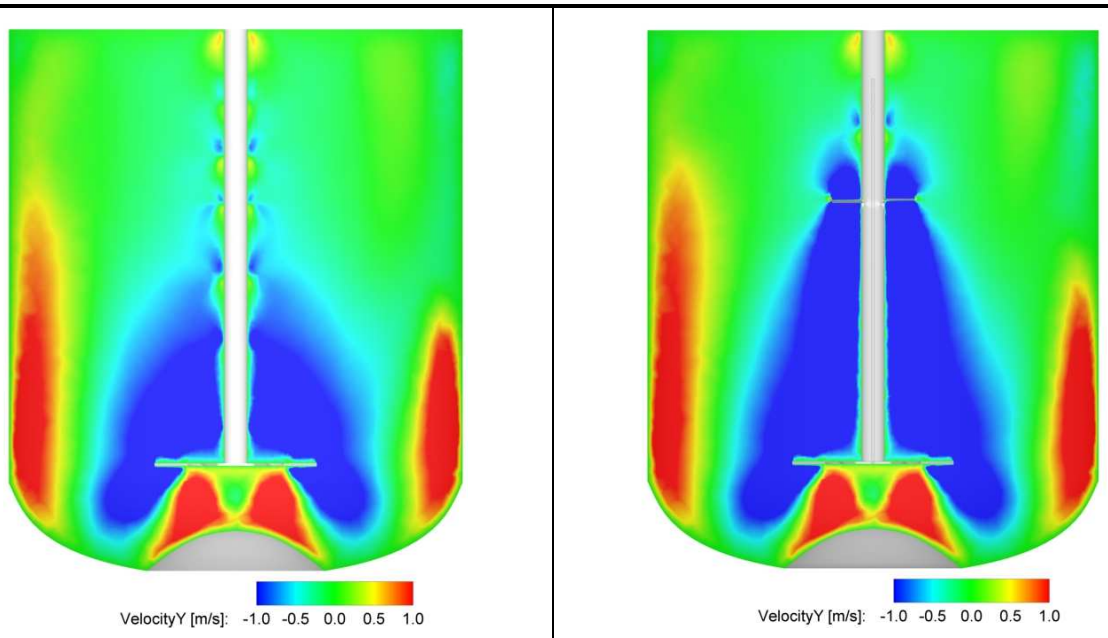

(a) (b)

Fig. 3.19 - Axial velocity, axial slice: a) Lower impeller configuration; b) Upper and lower impeller configuration.

By analyzing it, it is clear that the tank has lower axial velocities than the ones predicted on the Liquid case (Section 3.3.1.2). Yet, the effect of the upper impeller increases the downward velocity in the axis of the tank is clear, increasing the flow rate that passes in the lower impeller.

Also, on the impeller shaft some contour irregularities are noticed, especially for the lower impeller configuration. Probably this is due to the grid created around the shaft. Usually to economize grid elements while meshing a given volume, one can create a coarser grid near some less important zones, without losing accuracy on the final results. However in this case the grid near the shaft should be more refined so that those contours can be eliminated or explicated.

Figure 3.20 represents slices at different axial positions along the tank height. The upper impeller effect is notorious. Around the upper impeller the axial velocity is clearly negative enhancing the main axial loop in the tank.

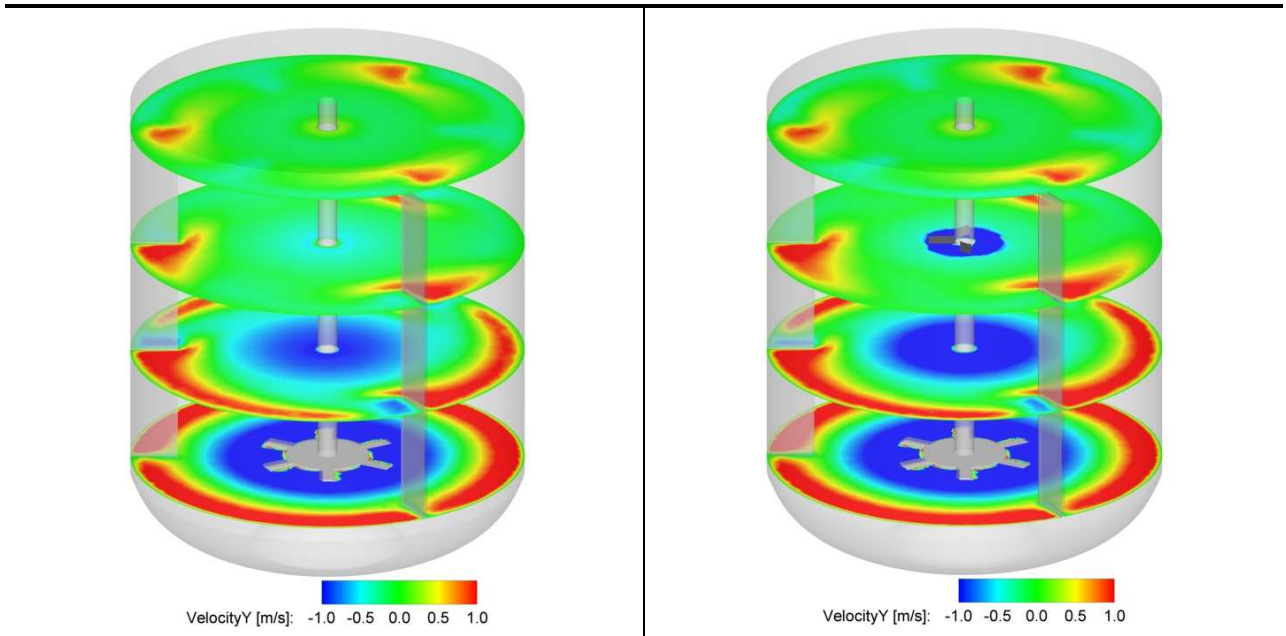

(a)	(b)

Fig. 3.20 - Axial velocity, represented at slices at different axial positions: a) Lower impeller configuration; b) Upper and lower impeller configuration.

Observing the second slice (looking upward), the region with negative velocities has a smaller propagation on the upper configuration than on the lower configuration.

Consequently the same conclusion can be extracted to the positive axial velocities regions. From the third slice up, there is only a slight enhancement on the axial velocity and therefore, a small mixing improvement can be achieved in this case.

3.3.2.3 Turbulent Kinetic Energy

The predicted turbulent kinetic energy contours are shown in Figure 3.21, for both impeller configurations. It is clear from both images that the effect on the fluid turbulent kinetic energy is, in this case, very significant. At this point it should be reminded that the quality of the mixing can be assured by analyzing the relative distribution of the turbulent kinetic energy (D.A. Deglon, 2006). Even though the magnitude of the turbulent kinetic energy near the upper impeller does not reach the correspondent magnitude on the lower impeller, the inherent improvement is notorious.

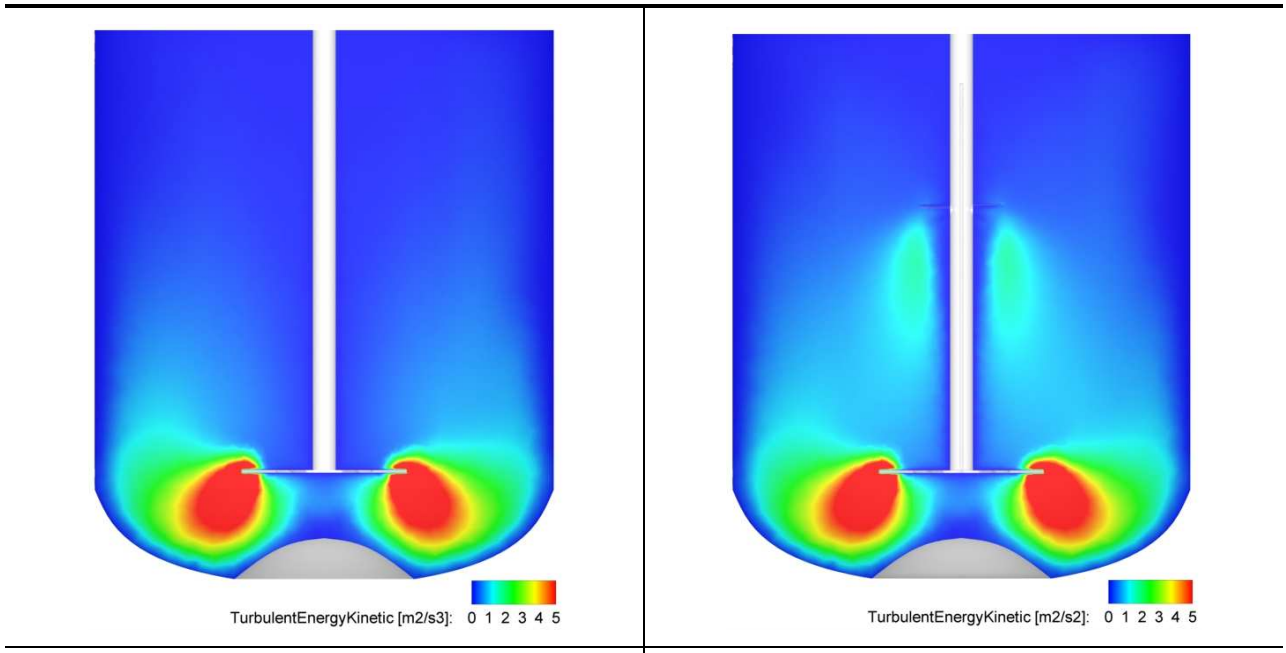

(a)	(b)

Fig. 3.21 - Turbulent Kinetic Energy, axial slice: a) Lower impeller configuration; b) Upper and lower impeller configuration.

Again, the upper impeller type is not adequate to stir up high viscosity loads. Therefore high turbulent kinetic energies were not expected for the region near the upper impeller. Preferably the fluid should have a defined downward flow, in that region of the tank, enhancing the main loop avoiding the appearance of stagnated regions.

This situation becomes clearer when looking at Figure 3.22.

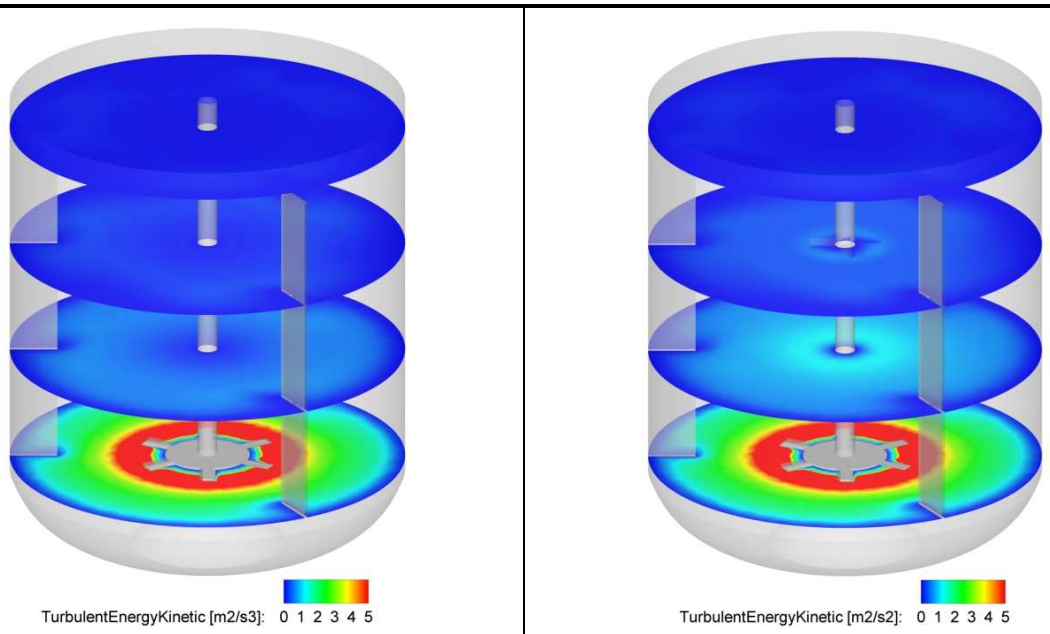

(a)	(b)

Fig. 3.22 - Turbulent Kinetic Energy, represented at slices at different axial positions: a) Lower impeller configuration; b) Upper and lower impeller configuration.

3.3.2.4 Turbulent Intensity

Figure 3.23 shows the effect of both impeller configurations.

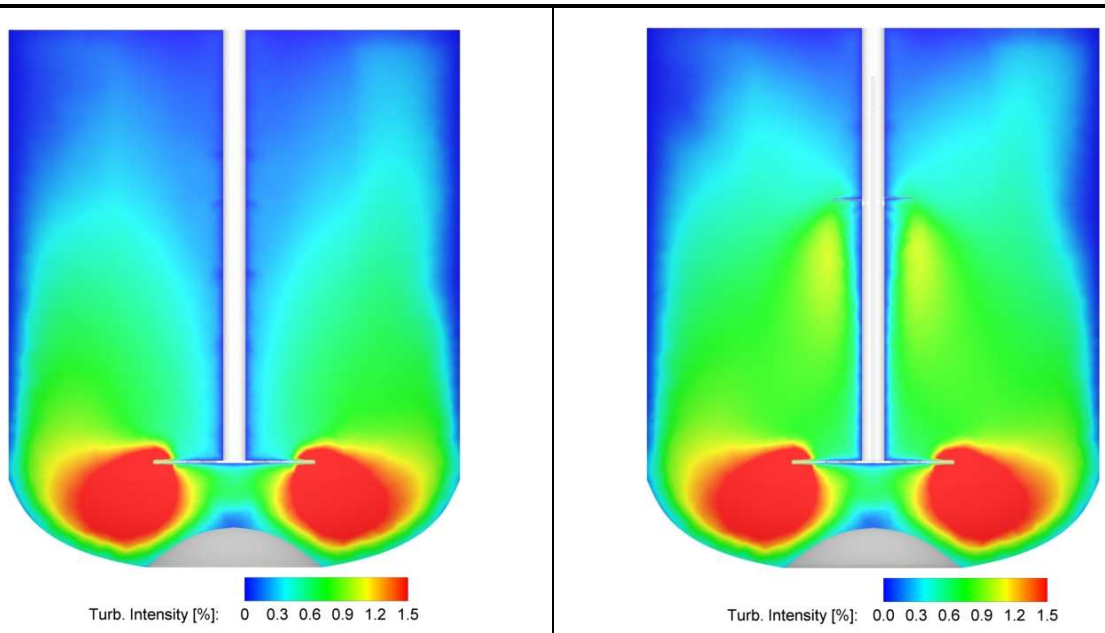

(a)	(b)

Fig. 3.23 - Turbulent Intensity, axial slice: a) Lower impeller configuration; b) Upper and lower impeller configuration.

Contrary to with the Liquid case (Section 3.3.1.4), where the turbulent intensities were uniform along the tank height, the Base case embraces the whole range of turbulent intensities. As expected the higher values are located near the lower impeller. However, for this case, the region on which the turbulence generated on the lower impeller has a bigger domain, extending high turbulences to whole bottom of the tank.

Although no direct conclusion should be taken into account without performing further studies, the turbulence intensities near the bottom of the tank, should be committed to their effect on the main loop. High turbulences near the bottom are necessary so that the accumulation of TiO_2 particles does not occur. However the axial velocity should be maintained impelling, in an ideal case, impelling these particles to flow all over the stirred tank, enhancing the final mixing quality.

Figure 3.24 provide an overall view of the turbulent intensity along the tank height and width. Attending to the first slice (looking upward) no significant difference was found between the both impeller configurations.

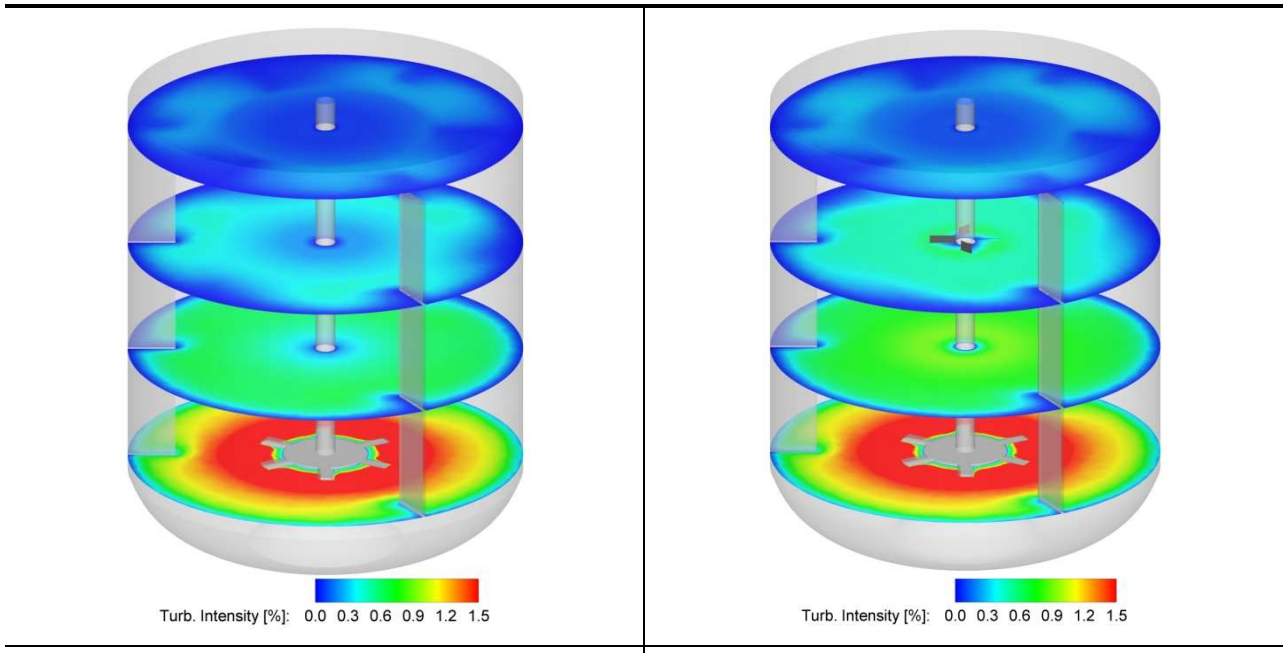

(a)	(b)

Fig. 3.24 - Turbulent Intensity, represented at slices at different axial positions: a) Lower impeller configuration; b) Upper and lower impeller configuration.

But comparing from the second slice until the top of the stirred tank, the turbulent intensity is clearly higher on the upper impeller configuration, turning slightly turbulent volumes into regions of significant turbulence and therefore mixing quality.

3.3.2.5 Power

The predictions of the power needed for both impeller configurations are shown on Table 3.10. For the lower impeller configuration the power predicted was P_{FLUENT} = 109.3 kW, 98.7% more power than the maximum power achieved by the stirred tank rotor.

Table 3.10 - FLUENT predicted results for the two impeller configurations.

ρ [kg/m³]	μ [$Poise$]	N [rpm]	Impeller Configuration	M_{imp} [N.m]	P_{FLUENT} [kW]	P_{SunChe} [kW]	Impeller power effect
1350	17	1460	lower impeller	715.8	109.3 (+ 98.7%)	55	-
1350	17	1460	lower and upper impeller	773.3	118.2 (+ 114.9%)	55	+ 8.1%

For the lower and upper impeller configuration the power predicted was P_{FLUENT} = 118.2 kW, 114.9 % more power than the maximum power achieved by the stirred tank rotor. Again the power is clearly over predicted. The explanation to these results can be extracted from the Liquid case. However, in relative terms, the upper impeller only increases about 8% the motor power, which is still higher than the 3% available.

The difference between the two impeller configurations becomes clearer with the increase of the fluid viscosity.

Due to the visible increase of mixing quality and to the low increase in the motor power, it was suggested to SunChemical to test the introduction of the upper impeller. According to Sunchemical feedback, there is a motor shut-off when the TiO_2 big-bag is added, due to the suden increase in viscosity. After starting it again it keeps working, due to the velocity variation it has on the start-up which limits the power. It was also mentioned that an increase on the product quality was observed, although it is still lower than that obtained from another company.

4 Conclusion

This research must be considered as a first approach to this particular stirred tank.

The flow patterns along the stirred tank for both loads are in a qualitative agreement with the patterns expected and so they should be used in further studies on this problem.

The predicted power was in all the simulations, higher than the measured power.

The results were severely constrained due to the unrealistic assumption of isotropic viscosity.

The 1.5 kW of input available will probably not be sufficient to implement another realistic impeller even if the FLUENT results represent correctly the stirred tank in study.

Better results would be achieved if more time was available to perform additional studies on the viscous models, on the viscosity dependence with temperature and shear rate and on the grid refinement.

The implementation of the upper impeller was tested being validated the increase in mixing quality, although there was a power shut-off of the motor, which had to be re-started. Additional time should be given to perform the correct approach to this problem. This project will continue between Fluidinova and Sunchemical, being by this time in study the possibility of changing to a more powerful motor or perform additional geometric changes in the tank geometry.

5 Evaluation

5.1 Objectives Accomplished

The objective of this work is to analyze a stirred tank and perform an initial study the effect of a second impeller on the enhancement of the solid/liquid mixture by analyzing the flow patterns and their effect on the power consumption.

Based on the powers predicted, the results should be taken into account in qualitative way and therefore the main objectives were accomplished. The simulations performed were able to establish a basic understanding of the process hydrodynamics and qualitative effect on the power required for different loads for the actual stirred tank. However, since there was no available time to study a non-Newtonian fluid, no valid quantitative results were found and therefore this research should be classified as a qualitative approach to this problem. Again, the implementation of a second impeller is not feasible based on the obtained results. Nevertheless Sunchemical was able to improve the final quality of mixing experiencing, however some power problems.

The author was also involved in a project for another company, Laborial. This project objective is to design a new fume cupboard using CFD analysis to certificate and enhance the exhaust flow patterns along the fume cupboard. Collaboration in this project has been a strong learning experience with an imperative impact on Laborial.

The training experience provided by Fluidinova was extremely important and should be stated. The author received intensive formation on ANSYS software Gambit 2.3.26, Fluent 6.3.26 and Tecplot 360 2008.

5.2 Limitations and impending work

These realized studies should be taken into account in a qualitative manner. The first approach to this project was performed assuming a value of 1100 rpm for the rotational speed and 25 Poise for the load's viscosity. Using these values, the dissipated power obtained by simulation was within the range of the potential power developed by the rotor. When these values were updated (1460 rpm and 0.946 and/or 14 Poise), the dissipated power obtained by each simulation was clearly over-predicted. In some cases, the dissipated power achieved three times the design value. It was clear that the model used on this work did not represent the real stirred tank in a quantitative manner. This is mainly due to several limitations imposed in this work as well as my on limitations on the software:

A. Usually industrial paints are non-Newtonian fluids. This means that the shear stress is not linearly related with the shear rate. In this case, the paint is a shear thinning fluid, which means that the apparent viscosity decreases with increasing shear rate – the harder the fluid is sheared, the less viscous it becomes. Additionally, the viscosity provided by SunChemical was obtained by measuring the slip time of the load through a cup, at the end of the stirring process. This viscosity corresponds to an average viscosity in the stirred tank. At this point, it must be considered that the region influenced by the impeller can be estimated. As mentioned on the state of the art, experiments have shown that the region where flow is strongly influenced by the periodic passage of the blades extends to a radius of D/2 away from the impeller tip and 1.5 blade heights above and below the impeller disk. So, in this region, the load's viscosity is below the average viscosity measured, making possible the 1460 rpm rotational speed at 53.5 kW of dissipated power. However, beyond this region the load has a higher viscosity and therefore its velocity is increasingly lower as we approach both the top and the tank walls.

B. The turbulence models chosen are not valid in the near wall region. Fluent has tools to fully describe the near wall phenomena. Because it is impractical to fully resolve the boundary layer or near wall effects, FLUENT uses a semi-analytical approach to determine near-wall effects (ex. Shear stress, convective heat transfer coefficient). These effects are modeled by near-wall relations or wall functions. One of the most common is Enhanced Wall Treatment function, used as a wall boundary condition mainly because the other near-wall modeling options did not took into account the turbulent effect on the sub-layer. Yet, in order to achieve valid results, this wall boundary condition requires a fine near-wall mesh capable of resolving this viscous sub-layer (more than 10 cells within the inner layer). To provide a quick answer to the problem presented, the grid was not excessively refined. The mesh refinement should be object of a deeper study in order to check the accuracy of the wall function, which would not be possible in the time frame of this project.

C. Further studies which combine experimental and computational investigations are needed to evaluate the influence of turbulence models (and grid refinement near the blades of the impeller) on the predicted characteristics of trailing vortices and on the flow field within the blades.

D. Further studies should be made in order to define the correct viscosity. Experimental measurements should be performed to understand the non-newtonian power law of the paint studied. Also, FLUENT has the capability of defining with the temperature and with the shearing stress. For example the Carreau Model can be applied as first approach.

E. Further studies should be made to determine the residence time of the fluid particles. An User Defined Function, UDF, could be created in FLUENT

F. Unfortunately the time available to perform this study was not sufficient. All the future work stated above strongly depends on the available time.

Despite the limitations presented, efforts were made to fulfill the objectives within the time available to execute the project, providing a useful and valid answer to given problem.

5.3 Remarks and Final Evaluation

The work done during this five month internship was more than worthwhile. I was expecting to undertake completely new software in a beautiful area of knowledge. Understanding some of most delicate aspects of computational fluids dynamics encouraged me to enhance my own engineering skills. I hold myself to this new step in my Chemical Engineer degree with all my courage and determination. The Fluidinova culture, the personal interaction, the day to day situations, the different job functions and especially the CFDapi dynamic attitude were essential to accomplish this complicated task.

As for the realized work, I have tried to provide sufficient information to understand and to define the specific role of computational flow dynamics on the stirred tank problematic, to select appropriate tools and models and, to apply them to link reactor geometry to reactor power performance. Although I am very pleased with the overall work potential as well as the possible impact of further studies on this thematic, the impossibility of future development within this internship process was difficult to accept.

6 References

Aubin J., F. D. (2004). Modelling turbulent flow in stirred tanks with CFD: the influence of modelling approach, turbulence model and numerical scheme. *Experimental Thermal and Fluid Science , 28*, pp. 431-445.

Bakker, B. &. (1994). Single-phase flow in stirred tanks. *Transactions of the Institution of Chemical Engineering , 72*, pp. 583-594.

Bartels C., B. M. (2002). Computational fluid dynamics applications on parallel-vector computers: computations of stirred vessel flows. *Computers & Fluids , 31*, pp. 69-97.

D.A. Deglon, C. M. (2006). CFD modelling of stirred tanks: Numerical considerations. *Minerals Engineering , 19*, pp. 1059–1068.

Hanjalic, K. L. (1980). Multiple time-scale concepts in turbulent transport modelling. *Turbullent shear flows , II*, p. 36.

J.Y. Luo, R. I. (1995). Prediction of impeller-induced flows in mixing vessels using multiple frames of reference. *8th European Conf. of Mixing* (p. 549). Cambrigde: IChem E Symposium.

K.H. Javed, T. M. (2006). Numerical simulation of turbulent batch mixing in a vessel agitated by a Rushton turbine. *Chemical Engineering and Processing , 45*, pp. 99-112.

Kader, B. (1981). Temperature and Concentration Profiles in Fully Turbulent Boundary Layers. *Int. J. Heat Mass Transfer , 24 (9)*, pp. 1541-1544.

Kim, J. (1978). Investigation of separation and reattachement of a turbulent shear layer: Flow over a backward facing step. *Ph.D. thesis* . Stanford University.

Kline, S. C. (1981). *The 1980-1981 AFOSR-HTTM - Stanford Conference on Complex Turbulent Flows* (Vols. I, II and III). Stanford University.

Launder, B. &. (1972). *Mathematical models of turbulence*. New York: Academic Press.

Launder, B. &. (1972). Prediction of free shear flows - a comparison of the performance of six turbulence models. *NASA* , SP 321.

Launder, B. &. (s.d.). The numerical computation of turbulent flows. *Computer methods in Applied Mechanics and Engineering , 3*, p. 269.

Ng, K. F. (1998). Assessment of sliding meshCFD predictions and LDA measurements of the flow in a tank stirred by a Rushton turbine. *Transactions of IChemE , 76*, pp. 737-747.

Pope, S. (1978). An explanation of the turbulent round-jet/plane-jet anomaly. *AIAA Journal , 16*, pp. 279-281.

Roback, R. &. (1983). Mass and momentum turbulent transport experiments with confined swirling coaxial jets. NASA CR-168252.

T. Kumaresan, J. B. (2006). Effect of impeller design on the flow pattern and mixing in stirred tanks. *115*, pp. 173–193.

Wechler, K. B. (1999). Steady and unsteady computations of turbulent flows induced by a 4/45° picthed-blade impeller. *ASME Journal of Fluids Engineering , 121*, pp. 318-328.

Z. Jaworski, K. D. (1997). The use of angle resolved LDA data to compare two different turbulence models applied to sliding mesh CFD flow simulations in a stirred tank. *Récents Progès en Génie des Procédés , 11 (51)*, pp. 187-194.

Z. Jaworski, W. B. (s.d.). CFD study of homgenisation with dual Rushton turbines - comparison with experimental results. *Trans IChem E , 78 A*, pp. 327-333.

7 Appendices

7.1 Case #1 - Rotational speed analysis

Usually when preparing the firsts simulations, the models used tend to be the one's provided by FLUENT defaults due to the uncertain associated to the tank's hydrodynamics. Thus, 1st order discretization scheme and standard $\kappa - \varepsilon$ were used on the first two simulations, prepared with 1100 rpm and with 1460 rpm.

The dissipated power was calculated by the product of the impeller moment, M_{imp}, with the impeller rotational speed, N. The impeller moment was obtained directly from FLUENT report moment menu. As an example for Case #1:

$$P_{FLUENT} = M_{imp} * N \tag{7.1}$$

$$P_{FLUENT} = \frac{689.6 \times 1100 \times 2 \times \pi}{60 \times 1000} \tag{7.2}$$

$$P_{FLUENT} = 79.4\ kW \tag{7.3}$$

The simulation results are shown in Table 7.1. Notice that these model over predicts the dissipated power in 44% for 1100 rpm and 214% for 1460 rpm. The effect of the impeller's speed is notorious. The increase of 360 rpm implies 93.3 kW of dissipated power.

Table 7.1 – FLUENT predicted results on the rotational speed variation.

ρ [kg/m³]	μ [Poise]	N [rpm]	Discretization Scheme	Viscous model	M_{imp} [N.m]	P_{FLUENT} [kW]	$P_{SunChemical}$ [kW]
1350	25	1100	1st order upwind	Standard $\kappa - \varepsilon$	689.6	79.4 (+ 44%)	55
1350	25	1460	1st order upwind	Standard $\kappa - \varepsilon$	1129.9	172.7 (+ 214%)	55

The near wall function has an important role on this discrepancy. Since the discretization scheme is of 1st order, the profile between each node is linear, which means that the turbulent effect is highly over predicted in the sub layer. Also, the grid near the impeller and the shaft is not optimized to the near wall function used, but it is extremely refined. Thus, for the following simulation second order upwind was used.

7.2 Case #2 – Discretization scheme analysis

In this simulation, a 2nd order discretization scheme was used to attenuate the unoptimized near wall function. The simulation results are shown in Table 7.2. Even though the model still over predicts the dissipated power, the power decrease is significant. For 1460 rpm the dissipated power decreased in 38 kW to 135 kW using a 2nd order discretization scheme. Further refinement on the discretization scheme was not considered, mainly because it would require more time and computational effort and also because the references found did not approach this thematic beyond the use of 2nd order discretization scheme.

Table 7.2 – FLUENT predicted results on the discretization scheme variation.

ρ [kg/m^3]	μ [Poise]	N [rpm]	Discretization Scheme	Viscous model	M_{imp} [N.m]	P_{FLUENT} [kW]	$P_{SunChemical}$ [kW]
1350	25	1460	1st order upwind	Standard $\kappa - \varepsilon$	1130	173 (+ 214%)	55
1350	25	1460	2nd order upwind	Standard $\kappa - \varepsilon$	885	135 (+ 146%)	55

At this point the path to improve the power results is defining a different turbulence model. In this case, two new simulations were prepared with the Realizable $\kappa - \varepsilon$ turbulence model.

7.3 Case #3 – Turbulence model analysis

The difference between the modeling of laminar and turbulent flows is the appearance of eddying motions of a wide range of length scales in turbulent flows. The standard $\kappa - \varepsilon$ is a semi-empirical model based on transport equations for the turbulent kinetic energy, κ and its

dissipation rate, ε. It perfoms poorly for complex flows involving strong streamline curvature, swirl, rotation, separating flows, etc.

The Realizable $\kappa - \varepsilon$ has a performance generally better than the standard $\kappa - \varepsilon$ model. It was chosen as the final turbulence model due to the combination of time interaction and its ability to describe accurately complex flow with large strain rates, predicting recirculations, rotations separations, etc.

Table 7.3 shows the results of the performed simulations.

Table 7.3 - FLUENT predicted results on the viscous model chosen.

ρ [kg/m^3]	μ [Poise]	N [rpm]	Discretization Scheme	Viscous model	M_{imp} [N.m]	P_{FLUENT} [kW]	$P_{SunChemical}$ [kW]
1350	25	1460	2nd order upwind	Standard $\kappa - \varepsilon$	885.2	135.3 (+ 146%)	55
1350	25	1460	2nd order upwind	Realizable $\kappa - \varepsilon$	817.2	124.9 (+ 127%)	55

By analyzing the results on the table, it is clear than even though the power is over predicted, the Realizable $\kappa - \varepsilon$ has a superior performance on power assessment than the standard$\kappa - \varepsilon$.